

# Pressure-annealed high-density amorphous ice made from vitrified water droplets: A systematic calorimetry study on water's second glass transition F SCI


Cite as: J. Chem. Phys. **157**, 064502 (2022); <https://doi.org/10.1063/5.0100571>


Submitted: 25 May 2022 • Accepted: 29 June 2022 • Accepted Manuscript Online: 15 July 2022 • Published Online: 11 August 2022

 Johannes Bachler,  Johannes Giebelmann,  Katrin Amann-Winkel, et al.

## COLLECTIONS

Paper published as part of the special topic on [Fluids Meet Solids](#)

 This paper was selected as Featured

 This paper was selected as Scilight



View Online



Export Citation



CrossMark

## ARTICLES YOU MAY BE INTERESTED IN

[Capture theory models: An overview of their development, experimental verification, and applications to ion-molecule reactions](#)

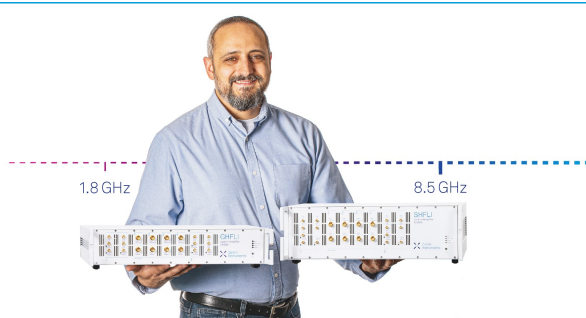
The Journal of Chemical Physics **157**, 060901 (2022); <https://doi.org/10.1063/5.0098552>


[Providing evidence for two remarkably stable liquid states in water](#)

Scilight **2022**, 331105 (2022); <https://doi.org/10.1063/10.0013688>

[Understanding the role of cross-link density in the segmental dynamics and elastic properties of cross-linked thermosets](#)


The Journal of Chemical Physics **157**, 064901 (2022); <https://doi.org/10.1063/5.0099322>





## Trailblazers.

Meet the Lock-in Amplifiers that measure microwaves.

 [Find out more](#)

# Pressure-annealed high-density amorphous ice made from vitrified water droplets: A systematic calorimetry study on water's second glass transition



Cite as: J. Chem. Phys. 157, 064502 (2022); doi: 10.1063/5.0100571

Submitted: 25 May 2022 • Accepted: 29 June 2022 •

Published Online: 11 August 2022



View Online



Export Citation



CrossMark

Johannes Bachler,<sup>1</sup> Johannes Giebelmann,<sup>1</sup> Katrin Amann-Winkel,<sup>2,3</sup> and Thomas Loerting<sup>1,a)</sup>

## AFFILIATIONS

<sup>1</sup>Institute of Physical Chemistry, University of Innsbruck, Innrain 52c, A-6020 Innsbruck, Austria

<sup>2</sup>Max-Planck-Institute for Polymer Research, Ackermannweg 10, 55128 Mainz, Germany

<sup>3</sup>Institute of Physics, Johannes Gutenberg University Mainz, Staudingerweg 7, 55128 Mainz, Germany

**Note:** This paper is part of the JCP Special Topic on Fluids Meets Solids.

**a) Author to whom correspondence should be addressed:** [thomas.loerting@uibk.ac.at](mailto:thomas.loerting@uibk.ac.at)

## ABSTRACT

In previous work, water's second glass transition was investigated based on an amorphous sample made from crystalline ice [Amann-Winkel *et al.*, Proc. Natl. Acad. Sci. U. S. A. **110**, 17720 (2013)]. In the present work, we investigate water's second glass transition based on the genuine glassy state of high-density water as prepared from micron-sized liquid water droplets, avoiding crystallinity at all stages. All the calorimetric features of water's second glass transition observed in the previous work are also observed here on the genuine glassy samples. This suggests that the glass transition indeed thermodynamically links amorphous ices continuously with deeply supercooled water. We proceed to extend the earlier study by investigating the effect of preparation history on the calorimetric glass transition temperature. The best samples prepared here feature both a lower glass transition temperature  $T_{g,2}$  and a higher polyamorphic transition temperature  $T_{ons}$ , thereby extending the range of thermal stability in which the deeply supercooled liquid can be observed by about 4 K. Just before the polyamorphic transition, we observe a spike-like increase of heat capacity that we interpret in terms of nucleation of low-density water. Without this spike, the width of water's second glass transition is 15 K, and the  $\Delta c_p$  amounts to  $3 \pm 1 \text{ J K}^{-1} \text{ mol}^{-1}$ , making the case for the high-density liquid being a strong liquid. We suggest that samples annealed at 1.9 GPa to 175 K and decompressed at 140 K to  $\geq 0.10 \text{ GPa}$  are free from such nuclei and represent the most ideal high-density amorphous glasses.

© 2022 Author(s). All article content, except where otherwise noted, is licensed under a Creative Commons Attribution (CC BY) license (<http://creativecommons.org/licenses/by/4.0/>). <https://doi.org/10.1063/5.0100571>

## INTRODUCTION

Water is abundant not only on Earth but also in space. While water on Earth can be encountered as ice, liquid water, or vapor, water in space is predominantly in an amorphous solid state.<sup>1,2</sup> When subjected to considerable pressure inside planets or moons, a wide range of solid high-pressure phases is accessible.<sup>3</sup> Bodies of liquid water, however, are limited to Earth and are considered a key requisite for the evolution of life. It is therefore not surprising that a vast amount of research has been devoted to understanding liquid water even under the most extreme conditions. This is not

an easy task, especially since water displays an impressive array of anomalies, including exponential increases in heat capacity and thermal compressibility upon supercooling.<sup>4,5</sup> There have been many attempts to explain the peculiar behavior of these thermodynamic response functions. Covering all of them to a sufficient extent is well beyond the scope of this work. Therefore, we would like to refer the interested readers to Refs. 4–7 for detailed reviews.

The scenario conjectured by Speedy<sup>8</sup> in 1982 has since been superseded by two-liquid models, such as the liquid–liquid critical point (LLCP) scenario<sup>9</sup> or the singularity-free scenario.<sup>10,11</sup> Especially the LLCP scenario has gained popularity in recent years

as it was confirmed in molecular dynamics computer simulations on full-atomistic water models, such as ST2,<sup>12</sup> TIP4P/2005, and TIP4P/Ice.<sup>13</sup> According to this scenario, the water separates spontaneously into two liquids, a high-density liquid (HDL) and a low-density liquid (LDL) at sufficiently low temperatures. These liquids exhibit a first-order liquid–liquid transition (LLT) that terminates at a second critical point. The heat capacity and compressibility anomalies are rationalized by approaching a critical point, which is known to lead to a divergence of response functions. In experiments, however, the existence of two distinct liquids and, consequently, the purported LLCP in water are hard to validate since they seem to be located below the homogeneous nucleation line  $T_H$  and above the (cold-)crystallization line  $T_x$ , where water crystallizes to ice in fractions of a second.<sup>14,15</sup> The LLCP can either be approached from above by cooling the supercooled liquid or from below by heating amorphous ices. This is because, in the framework of the LLCP hypothesis, low-density amorphous (LDA) ice and high-density amorphous (HDA) ice are believed to be the immobilized (=glassy) proxies related to LDL and HDL, respectively.<sup>6</sup>

LDA is often used as the generic term for amorphous ices with a density of 0.94 g/cm<sup>3</sup>.<sup>5,16–18</sup> It can be prepared either by vapor deposition,<sup>19</sup> rapid cooling of micron-sized water droplets (“hyperquenching”),<sup>20,21</sup> or heating of HDA at low pressures.<sup>22</sup> Since glasses are usually defined as vitrified liquids, LDA prepared via hyperquenching represents the most natural case for glassy low-density water. Upon reheating at 1 bar, this form exhibits a broad and feeble glass-to-liquid transition starting at around  $T_{g,1} = 136$  K,<sup>23–25</sup> which is interrupted by crystallization to ice I at around 150 K.<sup>26</sup>

HDA is commonly prepared via pressure-induced amorphization of ice I at temperatures below 140 K<sup>27,28</sup> and can be recovered to ambient pressure in a kinetically arrested state with density 1.15–1.17 g/cm<sup>3</sup>.<sup>16,28</sup> provided the temperature does not exceed ~100 K.<sup>29</sup> At low pressures, HDA transforms to LDA via an apparent first-order transition already at 105 K.<sup>22,30</sup> By subjecting HDA to pressure-annealing, its thermal stability toward LDA is greatly improved.<sup>31,32</sup> This more stable form of HDA is labeled eHDA (expanded HDA) and transforms to LDA at around 132 K at 1 bar.<sup>33</sup> Due to the improved thermal stability of eHDA, Amann-Winkel *et al.*<sup>34</sup> were able to identify a second glass-to-liquid transition at  $T_{g,2} = 115$ –116 K at 1 bar using calorimetry. After conversion to LDA at 132 K, they could even observe  $T_{g,1}$  at 136 K. In other words, two distinct glass transition phenomena, which are separated by ~20 K, are found in one single eHDA sample. This is a hallmark for liquid polymorphism, i.e., the existence of two different types of liquid water in a one-component system, and a necessary but not sufficient criterion for the LLCP hypothesis.

Recent pump–probe studies used IR laser-pulses to study amorphous water around ~200 K under slightly different conditions.<sup>35,36</sup> The authors of Ref. 36 employed a low-density amorphous ice sample heated transiently and stepwise through the underlying substrate. They found a gradual transition from high-density to low-density local structures during the subsequent cooling process from 245 to 190 K, monitored by IR-absorbance measurements. Instead, HDA was used as a starting material in Ref. 35, a free standing film of HDA was heated isochorically to a point in the phase diagram of a slightly elevated pressure around 205 K. The change in structure factors during the subsequent decompression (expansion) was

monitored using an x-ray free electron laser, and the authors observe a first-order phase transition before the intervention of crystallization, which they assigned to the high- to low-density liquid–liquid transition. Both datasets are consistent with transitions as predicted by the LLCP scenario.

These recent findings complement earlier studies on the behavior of supercooled water<sup>37–39</sup> and the melting lines of ice IV.<sup>40</sup> That is, water is one of the few one component substances where an LLT (associated with a second critical point) was suggested from experiments.<sup>33</sup> Nonetheless, these findings have been controversial, where it was argued that HDA is merely a collection of nanocrystals that results from the mechanical collapse of ice and that shows no resemblance to genuine glasses made by vitrification of liquid water.<sup>41–45</sup> Following this reasoning, HDA and, consequently, LDA made from HDA are not qualified to serve as the glassy proxies of HDL and LDL. Instead, the glass transitions  $T_{g,1}$  and  $T_{g,2}$  would be orientational glass transitions of crystals in which only rotational degrees of freedom thaw, but not true glass-to-liquid transitions in which translational degrees of freedom are also unlocked.<sup>46</sup> However, this hypothesis could not withstand ensuing scrutiny: Amann-Winkel *et al.*<sup>34</sup> found that the heat capacity increase at the glass transition of HDA is far too high (>4 J K<sup>-1</sup> mol<sup>-1</sup>) to be due to a simple orientational glass transition, which typically shows much smaller increases (~1 J K<sup>-1</sup> mol<sup>-1</sup>). Fuentes-Landete *et al.*<sup>47</sup> demonstrated that doping does not influence the dynamics of HDA and LDA near their glass transitions. By contrast, the dynamics at the orientational glass transitions in crystals, such as ice V, VI, and XII, are greatly enhanced by several orders of magnitude using suitable dopants. In our recent work, we showed that LDA made from liquid droplets undergoes a transition to a distinct amorphous form that is virtually identical to HDA in terms of thermal properties and x-ray diffraction pattern.<sup>48</sup> As there are no crystalline phases involved at any time in our experiments, these LDA and HDA states are guaranteed to represent the genuine glassy forms of two liquids. Still, key information about the nature of this second glass-to-liquid transition is missing. In particular, glass-to-liquid transitions are known to be strongly dependent on thermal history.<sup>49</sup> Already by altering the cooling rate, the temperature range where the liquid vitrifies is changed considerably. The pressure was also shown to have an effect on glass forming behavior, despite being mitigated in liquids with extensive hydrogen bonding.<sup>50</sup> Since LDA and HDA exhibit different hydrogen bonding,<sup>17,18</sup> they show a complex pressure-dependence of their  $T_g$ 's: While  $T_{g,1}$  (LDA) decreases with increasing pressure,  $T_{g,2}$  (HDA) increases with increasing pressure.<sup>51</sup> This is why Amann-Winkel *et al.* observed  $T_{g,2}$  around 115 K at 1 bar<sup>34</sup> whereas others observed  $T_{g,2}$  around 140 K at 1 GPa.<sup>52–55</sup> We emphasize that Amann-Winkel *et al.*<sup>34</sup> investigated  $T_{g,2}$  *ex situ* (after quench recovery) as opposed to the *in situ* studies in Refs. 52–55.

In this work, we tackle the question of whether high-density glasses that were prepared at different pressures differ in terms of their state of relaxation as expressed in terms of fictive temperature or excess entropy. In principle, it is desirable to attain the most relaxed states as they usually correspond to more stable glasses, which then exhibit a lower glass transition temperature. A lower  $T_{g,2}$  allows us to study a greater portion of the transformation range and possibly identify the end point where the fully mobile liquid is attained. For this reason, we subjected vitrified droplets

to a large variety of preparation protocols, including different initial compression-, annealing-, and decompression- (=relaxation) pressures in this work. Subsequently, the thermal behavior of high-density states at 1 bar is probed using differential scanning calorimetry (DSC) where significant effects regarding thermal stability and devitrification behavior are revealed.

Note that we named the HDA-like polymorph produced from vitrified droplets “densified hyperquenched glassy water” (d-HGW) and the LDA-like polyamorph “hyperquenched glassy water” (HGW) in our recent work.<sup>48</sup> This was done in order to distinguish them from the “traditional” amorphous ices made from crystalline ice and hence prone to the controversy that they are related to crystalline ice, not liquid water. For simplicity, we use the terms HGW/LDA and d-HGW/HDA interchangeably here. This is justified based on our earlier results on the topic<sup>48</sup> and is reinforced in the current study.

## EXPERIMENTAL DETAILS

### Sample preparation

The preparation of densified hyperquenched glassy water (d-HGW) closely follows the procedure reported in our earlier work.<sup>48</sup> First, HGW was prepared employing the setup of Kohl *et al.*<sup>24</sup> In short, a jet of finely dispersed aerosol of water droplets was generated and deposited onto a copper substrate cooled to 80 K. After 30 min of deposition, an HGW sample of roughly 2 mm thickness was obtained that could be recovered by immersing it together with the substrate in liquid nitrogen. Using a combination of x-ray diffraction (XRD) and differential scanning calorimetry (DSC), we determined the samples to be  $96\% \pm 4\%$  amorphous on average.<sup>48</sup> In other words, the samples are either fully glassy or mostly glassy with only minor contaminations of stacking disordered ice I.

Second, ~100 mg of HGW was scratched off the copper substrate, packed into an indium container, and transferred into our piston–cylinder setup, all while remaining under liquid nitrogen. Indium is indispensable in order to avoid frictional heating, which can transform amorphous ice into high-pressure ice modifications.<sup>56,57</sup> Force was then applied vertically using a material testing machine of Zwick Roell (model BZ100/TL3S). We used  $0.04 \text{ GPa min}^{-1}$  as the rate of compression and  $0.02 \text{ GPa min}^{-1}$  as the rate of decompression. Temperature stability of  $\pm 0.2 \text{ K}$  was achieved by combining the flow of cold gaseous nitrogen and resistive heating elements. Sample temperature was monitored using a Pt-100 sensor inserted into the compression cell. Heating rates were fixed to  $\sim 5 \text{ K min}^{-1}$ .

Third, the samples were high-pressure treated according to the scheme outlined in Fig. 1. Note that at pressures above 0.8 GPa, HGW converts fully to d-HGW even at 77 K.<sup>48</sup> Also note that ice  $I_h$  (used in most previous studies) converts fully to HDA at much higher pressures where typically 1.6 GPa is needed.<sup>28,34</sup>

### Variants of preparation protocols

We distinguish four different categories of preparation as shown in the individual panels (a)–(d). Following route (a),

the effect of the end pressure in the initial step (namely, the amorphous–amorphous transition from HGW to d-HGW at 77 K) is examined. That is, HGW is compressed to 1.1 GPa (black dot), 1.6 GPa (red dot), or 1.9 GPa (green dot) at 77 K, after which it is brought to 1.1 GPa. From there we follow the protocol of Ref. 32, i.e., the samples are isobarically heated to 160 K at 1.1 GPa, brought back to 140 K, and then decompressed isothermally. 140 K represents the upper temperature limit for decompression cycles where relaxation is as fast as possible, but crystallization to ice IX is still avoided.<sup>58</sup> We chose to stop the decompression at 0.10 GPa by quenching to 77 K and recovering to ambient pressure. This choice prevents back-conversion to HGW upon decompression.

In pathway (b), the influence of the second step, isobaric heating of d-HGW is probed. Samples subjected to this route are compressed to three different pressures and heated isobarically to just below the crystallization threshold:<sup>59,60</sup> 160 K at 1.1 GPa (black dot), 167 K at 1.6 GPa (red dot), and 175 K at 1.9 GPa (green dot). These  $p, T$  conditions are above the  $T_{g,2}$  line where the glass transforms into a highly viscous liquid.<sup>51</sup> Subsequently, the pressure-annealed d-HGW samples are cooled to 140 K back into the glassy state and decompressed isothermally to 0.10 GPa from where they are quench-recovered.

In routes (c) and (d), the effect of the third step, isothermal decompression of annealed d-HGW samples, is studied, more specifically of the end pressure, to which samples are quench-recovered. In (c), samples are compressed to 1.1 GPa, heated isobarically to 160 K, and decompressed isothermally at 140 K to 0.08 GPa (black dot), 0.10 GPa (red dot), 0.15 GPa (green dot), and 0.20 GPa (blue dot) and 0.25 GPa (cyan dot). The difference between (c) and (d) is that samples are compressed to 1.9 GPa and heated isobarically to 175 K in (d) rather than at 1.1 GPa to 160 K. The decompression step at 140 K is the same for both. According to Seidl *et al.*,<sup>54</sup> the samples turn into the highly viscous liquid between 0.20 and 0.10 GPa at 140 K [see the dashed line in Fig. 1(b)]. All samples are quench-recovered to 77 K and 1 bar after reaching the end pressure.

### Calorimetric analysis

Finally, quench-recovered pressure-annealed d-HGW was characterized *ex situ* at 1 bar using differential scanning calorimetry (DSC) and the procedures outlined in our earlier publications.<sup>33,48,61</sup> In short, we used a DSC8000 by PerkinElmer where the temperature calibration was carried out using indium, adamantane, and cyclopentane for heating/cooling rates of 10 and 30  $\text{K min}^{-1}$ . After carefully removing the indium encasing the sample, about 10–20 mg was transferred into an aluminum crucible and loaded into the pre-cooled instrument. *Ex situ* thermal analysis was performed between 93 and 300 K. Since it is not possible to weigh the samples under liquid nitrogen, the scans are normalized using the melting enthalpy of ice of  $6012 \text{ J mol}^{-1}$  at 273 K [see the supplementary material (Fig. S1) for details]. A second heating scan of ice serves as a baseline. Onset temperatures are obtained by the intersection of the baseline with a tangent adjusted to the calorimetric event. Each sample was measured at least two times. Transition temperatures within a sample batch are resolved with an accuracy of  $\pm 0.2 \text{ K}$ . Transition temperatures between different sample batches were determined to have an uncertainty of  $\pm 1 \text{ K}$ . Unless stated otherwise, the latter uncertainty was used for plotting error bars.

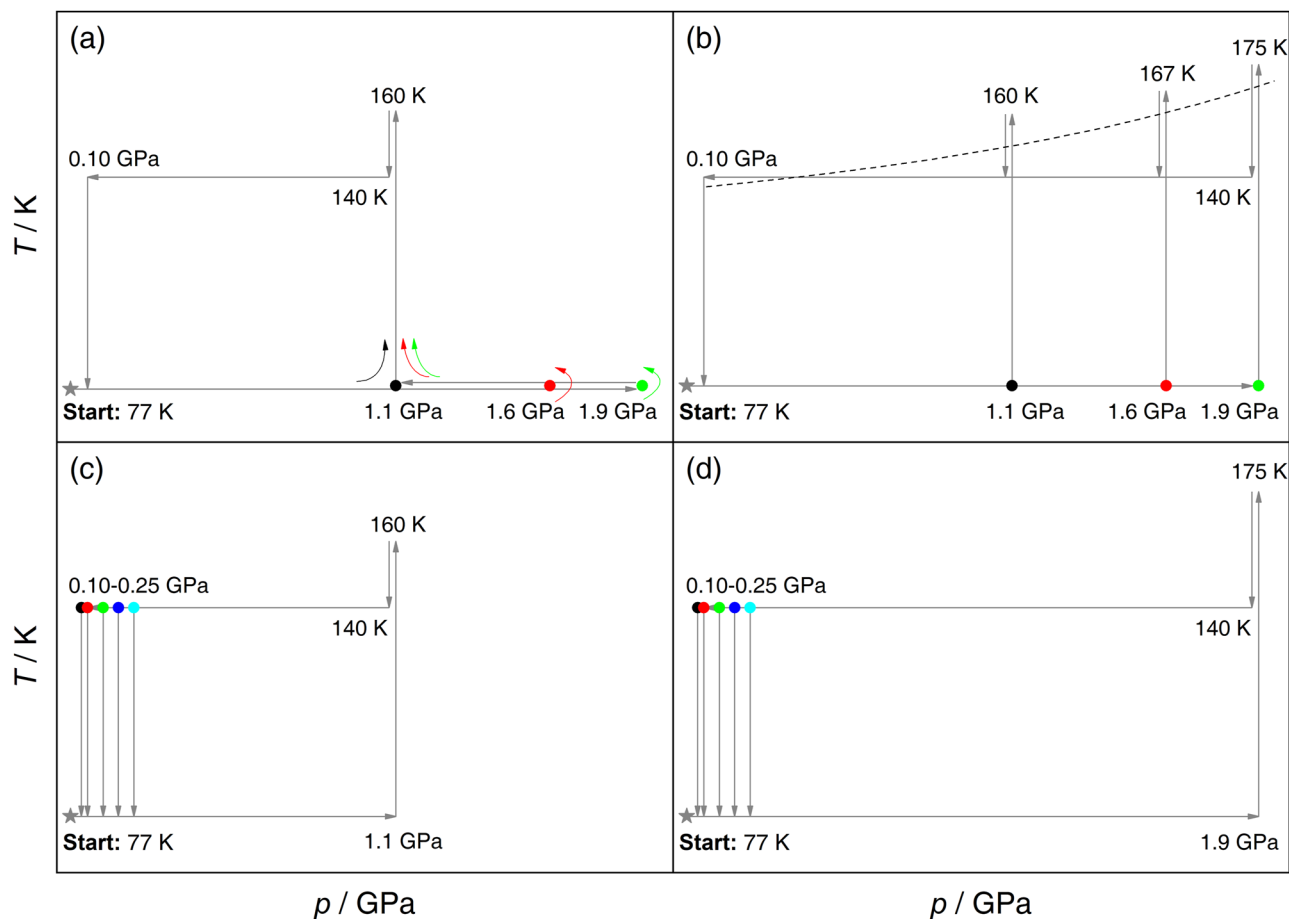


**FIG. 1.** (a)–(d) Scheme of four types of  $p$ – $T$  protocols used in this work for preparing d-HGW from HGW as the starting material. The  $T_{g,2}$  line of HDA/HDL from Ref. 6 is indicated as a black dashed line in (b). In our preparation protocols, it is always crossed upon isobaric heating and sometimes during decompression at 140 K (only <math><0.20\text{ GPa}</math>).<sup>54</sup>

## RESULTS AND DISCUSSION

In the first section, we will discuss the impact of the different preparation protocols on the polyamorphic HDA  $\rightarrow$  LDA transition. In the second section, we will focus on the second glass transition related to the HDA  $\rightarrow$  HDL transition and associated phenomena taking place in this temperature range.

### The polyamorphic HDA $\rightarrow$ LDA transition at 1 bar

Figure 2 shows a selection of DSC heating scans of pressure-annealed HDA where the arrangement of panels (a)–(d) exactly matches the arrangement of panels in their preparation pathways displayed in Fig. 1. All scans are dominated by the pronounced exotherm at  $135 < T < 145\text{ K}$ , which represents the heat released for the sharp first-order-like HDA  $\rightarrow$  LDA transition. At 147 K, i.e., after completion of this transition, the samples are cooled back to 93 K and then reheated to 300 K. In this second heating scan, the crystallization of LDA to stacking-disordered ice  $I_{sd}$  and the polytypic

conversion of ice  $I_{sd}$  to ice  $I_h$  are observed [see the [supplementary material](#) (Fig. S1)].<sup>48</sup>

As described in the work by Winkel *et al.*,<sup>33</sup> the location of the HDA  $\rightarrow$  LDA transformation peak can be employed to assess the degree of relaxation. Their most relaxed samples (“eHDA”) show a peak temperature  $T_{min}$  of 134 K, whereas the least relaxed samples (unrelaxed HDA, “uHDA”) show a much lower  $T_{min}$ , namely, 117 K. In addition to  $T_{min}$ , we extracted the onset temperatures  $T_{ons}$  of the transition. The latter is known to be less rate-dependent.<sup>62</sup> Results of this analysis are shown in Fig. 3, where  $T_{ons}$  is represented by filled circles and  $T_{min}$  by filled squares.

In general, both onset  $T_{ons}$  and peak temperature  $T_{min}$  show similar trends albeit being separated by roughly 2 K. Panel (a) shows the impact of initial compression pressure on the transition temperatures. This effect could not be considered in previous studies because traditional HDA only forms at pressures above 1.2 GPa when compressing ice I at 77 K.<sup>28</sup> Our data reveal that this effect is negligible and transition temperatures remain around  $T_{ons} = 139\text{ K}$  and  $T_{min} = 141\text{ K}$ . That is, there is no difference whether LDA



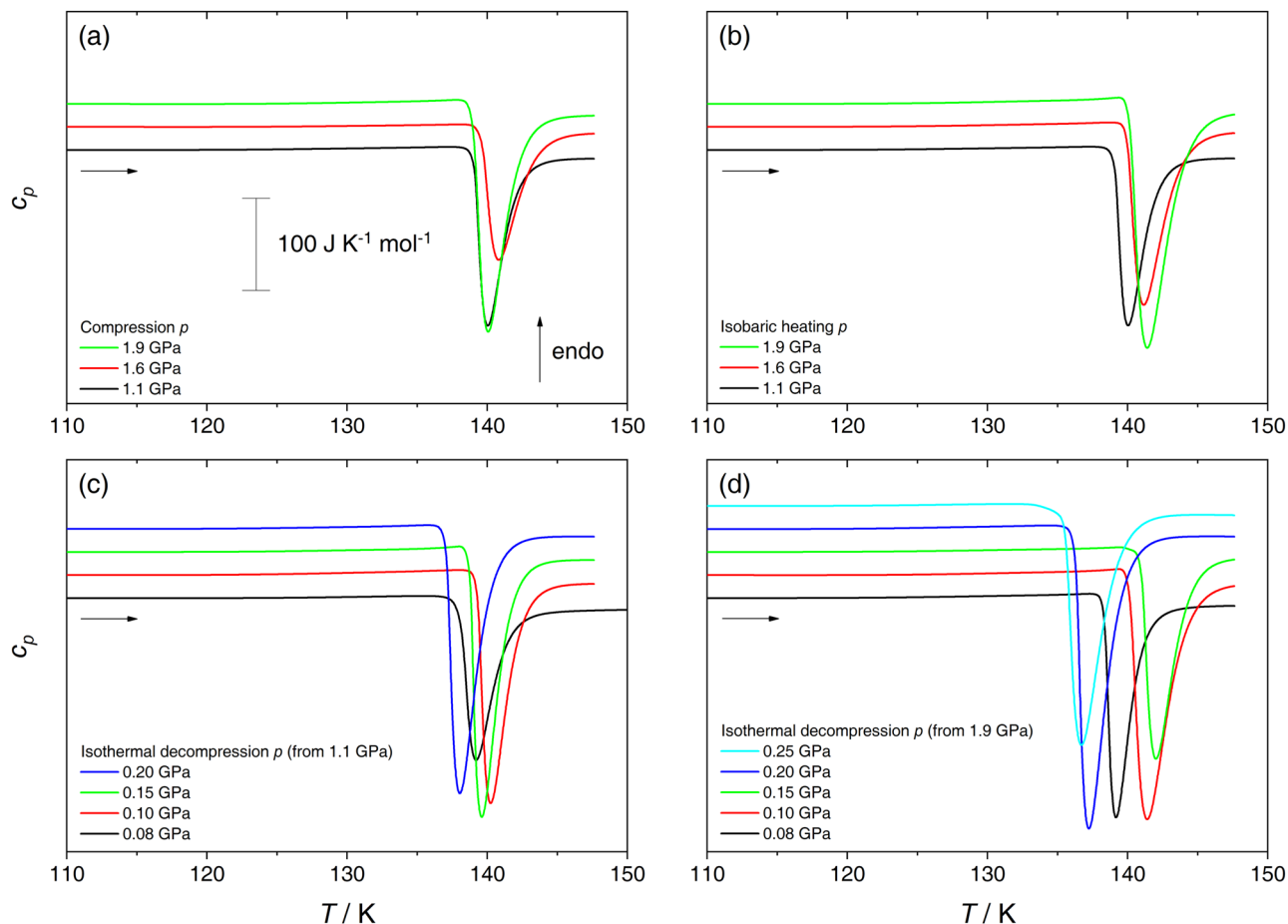


**FIG. 2.** (a)–(d) Heating thermograms of d-HGW samples subjected to the routes (a)–(d) in Fig. 1 with a focus on the exotherm indicating the polyamorphic transition. Traces are recorded at 1 bar with heating rates of  $30 \text{ K min}^{-1}$ . Curves are shifted vertically for clarity.

is compressed to the minimum pressure required to form HDA (e.g., 1.1 GPa) or well beyond (e.g., 1.9 GPa). A similar observation is made for the isobaric heating step as indicated in panel (b) with a slight increase at high pressure:  $T_{\text{ons}}(1.1 \text{ GPa}) = 139.3 \text{ K}$  and  $T_{\text{ons}}(1.9 \text{ GPa}) = 139.9 \text{ K}$ . However, this increase is close to the reproducibility of our DSC experiments (typically on the order  $\pm 1 \text{ K}$ ). That is, the first two steps, compression at 77 K and pressure-annealing at high temperatures close to  $T_x$ , do not impact much on the onset temperature.

However, the third step, isothermal decompression, has a considerable effect on transformation temperature as shown in Fig. 3(c) and (d). The thermal stability of HDA against transformation to LDA increases with decreasing pressure from 0.20 to 0.10 GPa. This implies that HDA relaxes more and more upon decompression at 140 K, as also noted earlier for the eHDA samples.<sup>33</sup> Interestingly, HDA quench-recovered at 0.08 GPa no longer follows this trend but transforms at lower temperatures. While this observation was made earlier, at that time it lacked a conclusive explanation.<sup>63</sup> Recent findings about peculiar crystallization behavior of

decompressed HDA samples by Tonauer *et al.*<sup>64</sup> help rationalizing this behavior: nanosized LDA domains nucleate near 0.15 GPa within the amorphous HDA matrix when decompressing at 140 K; these nuclei trigger ice IX crystallization under high pressure conditions and trigger LDA growth at the low-pressure conditions encountered in our DSC instrument. Based on this conjecture, two competing processes are relevant for the thermal stability of HDA at 1 bar: On one hand, HDA-relaxation stabilizes HDA toward LDA, but on the other hand, LDA nuclei destabilize HDA by facilitating the growth of LDA. Hence, we explain the findings in Figs. 3(c) and 3(d) as follows: At decompression pressures between 0.25 and 0.15 GPa, there is only relaxation of HDA, steadily increasing  $T_{\text{ons}}$ . Between 0.15 and 0.10 GPa, HDA further relaxes while some LDA nuclei form within the matrix. As the number of available nuclei is small,  $T_{\text{ons}}$  is still dominated by the relaxation effect, i.e., it is shifted to higher temperatures. Between 0.10 and 0.08 GPa, HDA is eventually well-relaxed but LDA nucleation is taking place more rapidly. Now, the number of nuclei is large enough to lower the thermal stability of HDA, despite HDA being relaxed even more at 0.08 GPa.

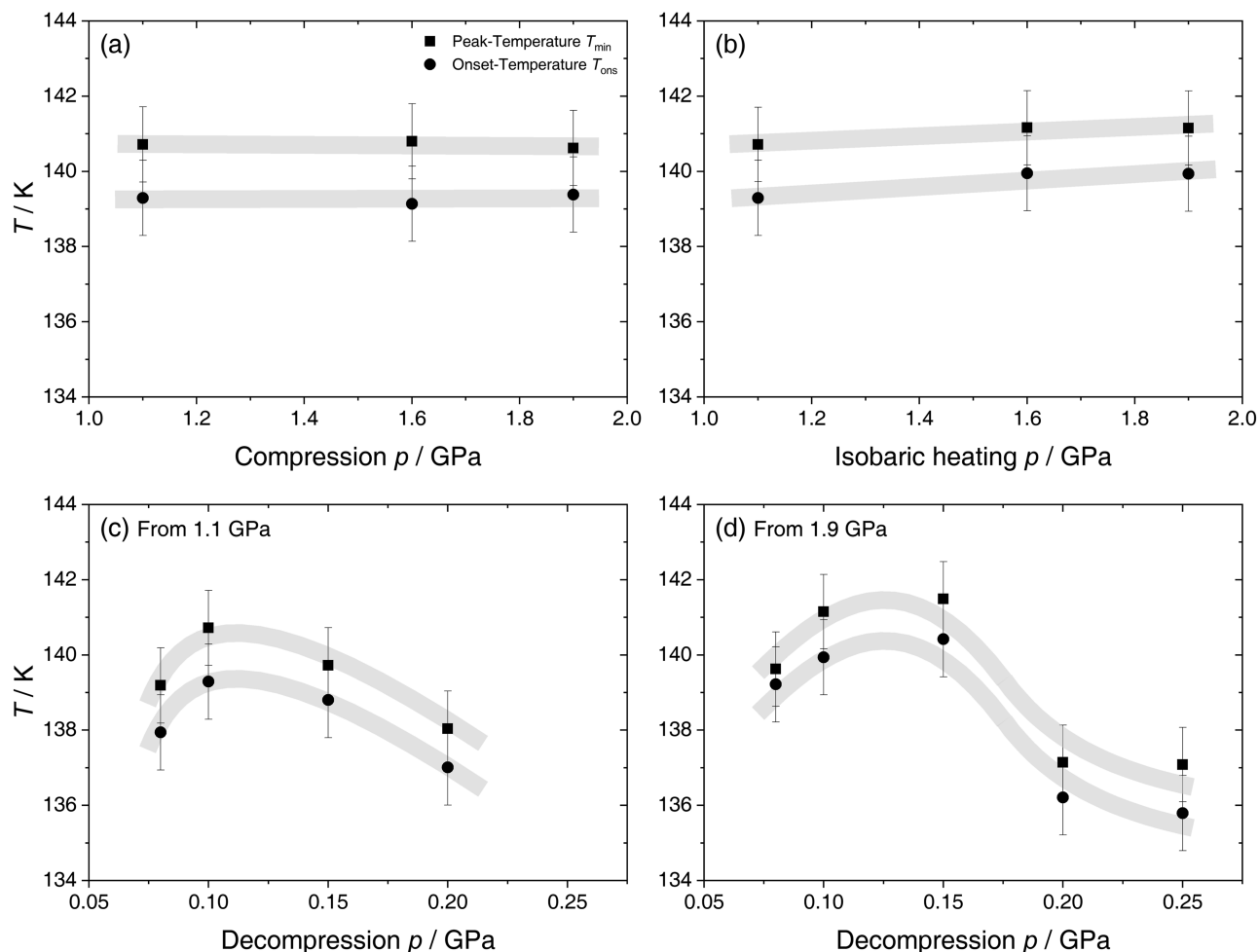


**FIG. 3.** (a)–(d) Polyamorphic (HDA  $\rightarrow$  LDA) transition at 1 bar of d-HGW produced via the routes shown in Figs. 1(a)–1(d). Filled squares represent peak temperatures  $T_{min}$  and filled circles onset temperatures  $T_{ons}$ . Broad gray lines are guides to the eye.

The comparison of Figs. 3(c) and 3(d) reveals that samples previously heated isobarically at 1.9 GPa are slightly more stable than samples heated at 1.1 GPa. This implies that they relax faster and LDA nucleation is suppressed or even both. As a result, the highest thermal stability at 1 bar of  $T_{ons} \sim 141$  K is reached already at a decompression pressure of 0.15 GPa. This is remarkably close to the quasi-equilibrium line between LDA and HDA, located at  $\sim 0.20$  GPa<sup>65</sup> Based on these observations, we claim that HDA samples heated at 1.9 GPa and decompressed to 0.10–0.15 GPa at 140 K display the highest thermal stability against the polyamorphic transition at ambient pressure.

For comparison, the HDA samples employed by Amann-Winkel *et al.*<sup>34</sup> convert to LDA already at  $T_{ons} \sim 132$  K. In order to account for the different heating rates employed in the calorimetry experiments by Amann-Winkel *et al.* ( $10$  K  $\text{min}^{-1}$ ) and us ( $30$  K  $\text{min}^{-1}$ ), we have measured one sample using several different heating rates [see the [supplementary material](#) (Fig. S2)]. This analysis suggests that the increase in heating rate from 10 to  $30$  K  $\text{min}^{-1}$

shifts the transition up by 4 K. That is, if Amann-Winkel *et al.*<sup>34</sup> had used a heating rate of  $30$  K  $\text{min}^{-1}$ , they would have found a transition temperature  $T_{ons}$  of 136 K. They prepared HDA by isobaric heating at 1.1 GPa and decompression to 0.08 GPa—we find  $T_{ons} = 138$  K for samples prepared using their thermodynamic path but starting from liquid droplets rather than ice  $I_h$ . That is, using these HDA samples and annealing them at 1.9 GPa extends the temperature window where HDA can be investigated at 1 bar by  $\sim 5$  K (from 136 to 141 K).

## The second glass transition

### The spike-like feature

Figure 4 shows a different magnification level of thermograms displayed in Fig. 2. Here, an endothermic event preceding the polyamorphic HDA  $\rightarrow$  LDA transition is observed for all samples. This increase in  $c_p$  was attributed to be the signature of the second

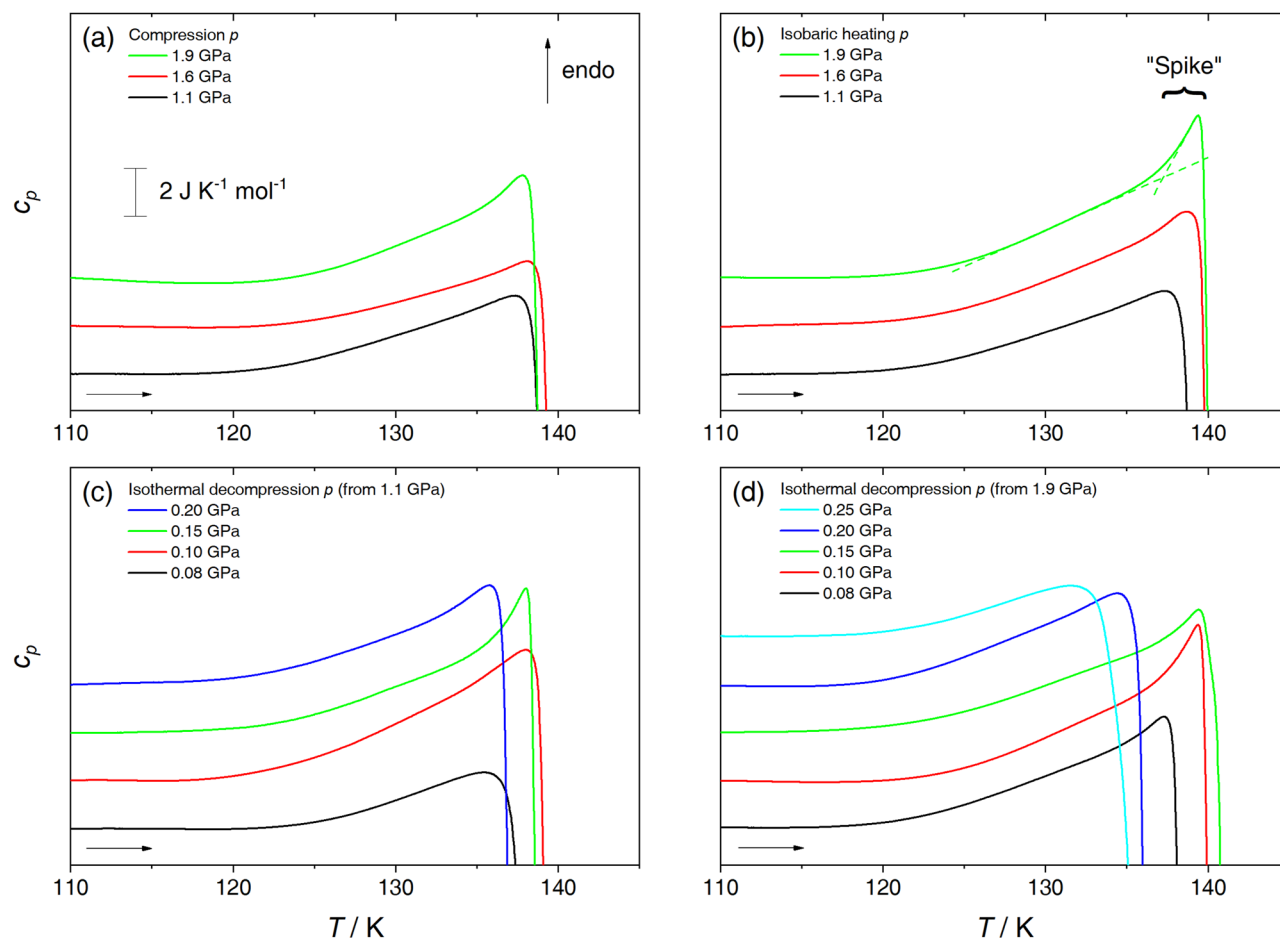


**FIG. 4.** (a)–(d)  $\sim 50$ -fold magnification of thermograms in Figs. 2(a)–2(d). Traces are recorded at 1 bar with heating rates of  $30 \text{ K min}^{-1}$ . An example of the spike-like feature is marked for the green curve in panel (b) by a curly bracket and placed tangents (dashed). Curves are shifted vertically for clarity.

glass-to-liquid transition where HDA transforms to HDL.<sup>34</sup> We note that the black trace in panel (c) is recorded from a sample that most closely corresponds to the one published in earlier work. Inspecting this trace, we find an almost linear increase in  $c_p$  starting at 124 K that ends with the sudden exothermic transformation to LDA. However, this is not the case for all our scans. Other scans [e.g., green curve in Fig. 4(c)] show a linear increase in  $c_p$  starting at 123 K, followed by a much steeper linear increase near 135 K. We call this latter feature the “spike” [as marked in Fig. 4(b)]. Such a feature was previously identified in some pure HDA pressure-annealed samples<sup>66</sup> but not all,<sup>34</sup> as well as in some HDA samples from aqueous solutions.<sup>66,67</sup> We now reveal under which conditions this spike is observed reproducibly. It always appears in samples that were decompressed to 0.15 GPa [green traces in panel (c) and (d)], no matter if originally treated at high or low pressures. For samples decompressed to 0.10 and 0.08 GPa, it appears for samples annealed at 1.9 GPa [green curves in panel (a) and (b), black and red curve in panel (d)], but is rarely observed in HDA that was treated at 1.1 GPa [black curves in panel (a) and (b), black and red curve in panel (c)]. By contrast,

in samples decompressed to 0.20 GPa, a (smaller) spike is observed only when annealed at 1.1 GPa but not at 1.9 GPa. That is, the occurrence of the spike seems to correlate with the thermal stability of HDA at 1 bar where it is more likely to be found in thermally stable samples (compare with Fig. 3). Upon closer inspection of the spike in Fig. 4, we find that blue, green, and red traces of (c) are remarkably similar to the green, red, and black curves in (d) regarding the occurrence of the spike. That is, the 1.1 GPa samples decompressed to 0.20 (or 0.15 or 0.10) GPa show largely similar behavior to 1.9 GPa samples decompressed to 0.15 (or 0.10 or 0.08) GPa. This could indicate that the spike is somehow linked to the degree of relaxation of HDA, which is reached at different stages in the decompression process, and would imply that the 1.9 GPa samples are less relaxed than the 1.1 GPa ones—the difference in relaxation then amounts to  $\sim 0.05$  GPa on the decompression path. However, this is contradicted by the higher polyamorphic transformation temperature of the former samples [the difference  $\Delta T_{\text{ons}}$  for the 0.15–0.08 GPa samples in Figs. 3(c) and 3(d) is 1.0–1.7 K], which implies increasingly relaxed HDA when annealed at 1.9 GPa.



Consequently, explaining the spike-like feature is a task, which seems to require a more complex approach.

Two explanations were originally put forward to explain the spike in HDA containing LiCl, (i) unfreezing of translational modes of water molecules and (ii) adiabatic cooling incurred upon the 25% density decrease associated with the polyamorphic transition,<sup>66</sup> but both show significant caveats. Idea (i) that rotation modes thaw during the initial part of the glass transition and translational modes during the spike is in conflict with the results of Perakis *et al.*,<sup>68</sup> who show that diffusion already occurs at temperatures as low as 132 K. Idea (ii) that the sudden volume expansion by 25% resulting from the polyamorphic transformation induces an endotherm via adiabatic cooling does not provide any explanation why such an effect should start to occur slightly before the actual transformation. Hence, we want to suggest another possibility (iii): the spike indicates the nucleation of LDA/LDL droplets in HDL at 1 bar, which in turn initiates the polyamorphic transition (or the LLT).

We rationalize this as follows: As the spike always appears upon heating the thermally most stable samples (i.e., the ones made by annealing at 1.9 GPa), we presume that the spike is tied to HDA that exhibited little to no nucleation of LDA during the decompression process. The nucleation, however, then takes place during the scan in the calorimeter. In the simplified picture of classical nucleation theory, the formation of the new more stable phase within the metastable phase is always associated with an energy barrier. This barrier opposes the gain of free energy that would be achieved upon transforming to the new phase. In order to transform, some molecules must arrange into clusters of new phase by taking up enough energy to overcome the barrier (=nucleation). In the case of freezing water to ice below 0 °C, this is easily feasible as the thermal energy present in the system is sufficient to induce ice-like clusters through structural fluctuations. The new phase then grows rapidly thus releasing the full free energy of the phase transition (=growth). These two events can only be separated when employing ultrafast probing techniques. At temperatures as low as 136 K, dynamics slow down sufficiently to allow observing nucleation and growth as two distinguished events at timescales on the order of seconds. The endothermic spike would then correspond to nucleation whereas the ensuing exotherm corresponds to the growth of the LDL phase. This idea contrasts the idea that HDA transforms to LDA via spinodal decomposition at ambient pressure.<sup>69,70</sup> Spinodal decomposition may be the case under pressure for the polyamorphic transition upon decompression in the liquid state. In our experiment at 1 bar, starting from glassy HDA, rather nucleation and growth is the likely mechanism. In this context, we stress that up until now no pure HDA sample could be heated to temperatures this high in conventional calorimetric experiments, so that we might see signatures of nucleation only because of the high thermal stability of HDA made according to our protocol. We explain the development of the spike in more detail using the scheme shown in Fig. 5.

Figure 5 is a representation of the free energy landscape of HDA and LDA at 0.25 GPa, 0.15 GPa, and 1 bar. The landscape changes with changing pressure,<sup>71</sup> where decreasing the pressure from 0.25 to 0.15 GPa leads to a shift of the local HDA minimum, as more expanded states are preferred. When subjected to appropriate annealing protocols, HDA can be relaxed to a state very close to

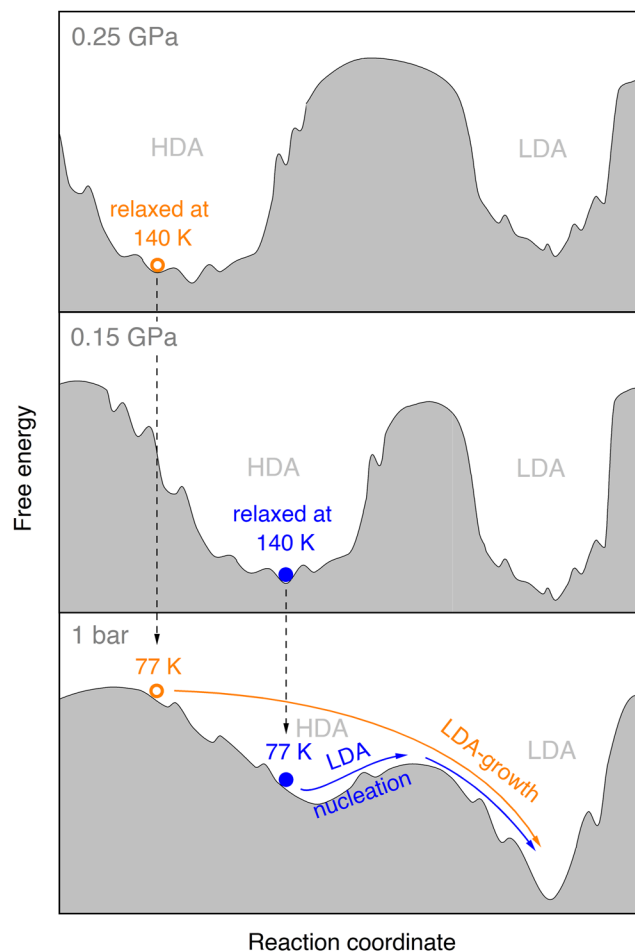


**FIG. 5.** Schematic representation of the energy landscape of HDA and LDA at 0.25 GPa, 0.15 GPa, and 1 bar. HDA states relaxed at 0.25 and 0.15 GPa are drawn as open orange and filled blue circles, respectively. After quench-recovery to 1 bar and 77 K, they remain in their high-pressure configuration (dashed black arrows). Upon reheating, they move toward an energetically more favored configuration, where HDA quenched at 0.25 GPa is highly unstable, directly transforming to LDA without energy barriers (orange arrow). HDA quenched at 0.15 GPa by contrast needs to overcome a nucleation barrier before LDA growth can take place (blue arrows).

the minimum of the basin. We achieve this equilibration by slow decompression at 140 K. The equilibration is completed quickly once HDA is in a sufficiently mobile state, i.e., close to its glass transition (around 0.20 GPa at 140 K). That is, at 0.25 GPa, HDA is rather close to the local minimum (open circle) and, at 0.15 GPa, it is in the local minimum (filled circle). Upon quenching to 77 K, the samples are trapped in the position of the energy landscape that they have attained during decompression. Yet, the landscape changes once again after recovery to 1 bar (sketched by arrows pointing into the lowest panel)—now LDA is the most stable amorphous state and HDA is highly metastable. The equilibrated configurations at high pressures now suddenly correspond to random state points in the increasingly broad basin of HDA states at 1 bar. Because they are

deeply frozen in their glassy states, they can no longer relax toward the “new” local minimum. That is, configurations that were the most stable at high pressures are now clearly far away from equilibrium, where, e.g., configurations from 0.25 GPa are further away than configurations from 0.15 GPa. Upon reheating at 1 bar in calorimetry, they proceed toward the energetically more stable states as soon as they are mobile enough, which is most certainly the case at  $T_{g,2}$ . The 0.25 GPa samples that are further away from the equilibrium configuration of HDA (=high excess energy) are high enough on the energy landscape to turn into the stable state LDA state without any energy barriers. This leads to the observation of a phase transition that shows little to no apparent activation barrier, i.e., it is reminiscent of spinodal decomposition. On the other hand, the 0.15 GPa samples are closer to the favored configuration of HDA at 1 bar, and they hardly gain energy from relaxation. Once they reach the glass transition temperature, they relax slightly and end up in the local minimum of HDA/HDL. Only at comparably high temperatures,

some domains have enough thermal energy to jump over the activation fence. We postulate that this jump is divided into the spike-like feature corresponding to nucleation (first blue arrow in Fig. 5) and the ensuing exotherm corresponding to growth (second blue arrow).

We now use this model with the purpose of explaining the presence and absence of the spike in scans of Figs. 4(c) and 4(d). In samples decompressed to  $>0.20$  GPa, HDA is not yet well-relaxed and transforms to LDA via spinodal-like decomposition. Consequently, no spike is observed and thermal stability is rather low. In samples decompressed to 0.15 GPa, HDA is well-relaxed and, therefore, highly thermally stable. In order to transform to a more stable low-density state, small nuclei are formed, initially consuming free energy and, hence, leading to heat capacity spikes. Finally, in samples decompressed to 0.10–0.08 GPa, LDA nucleation becomes more and more likely to occur during the decompression process. If LDA nucleates already during this step, it will no longer need to do so

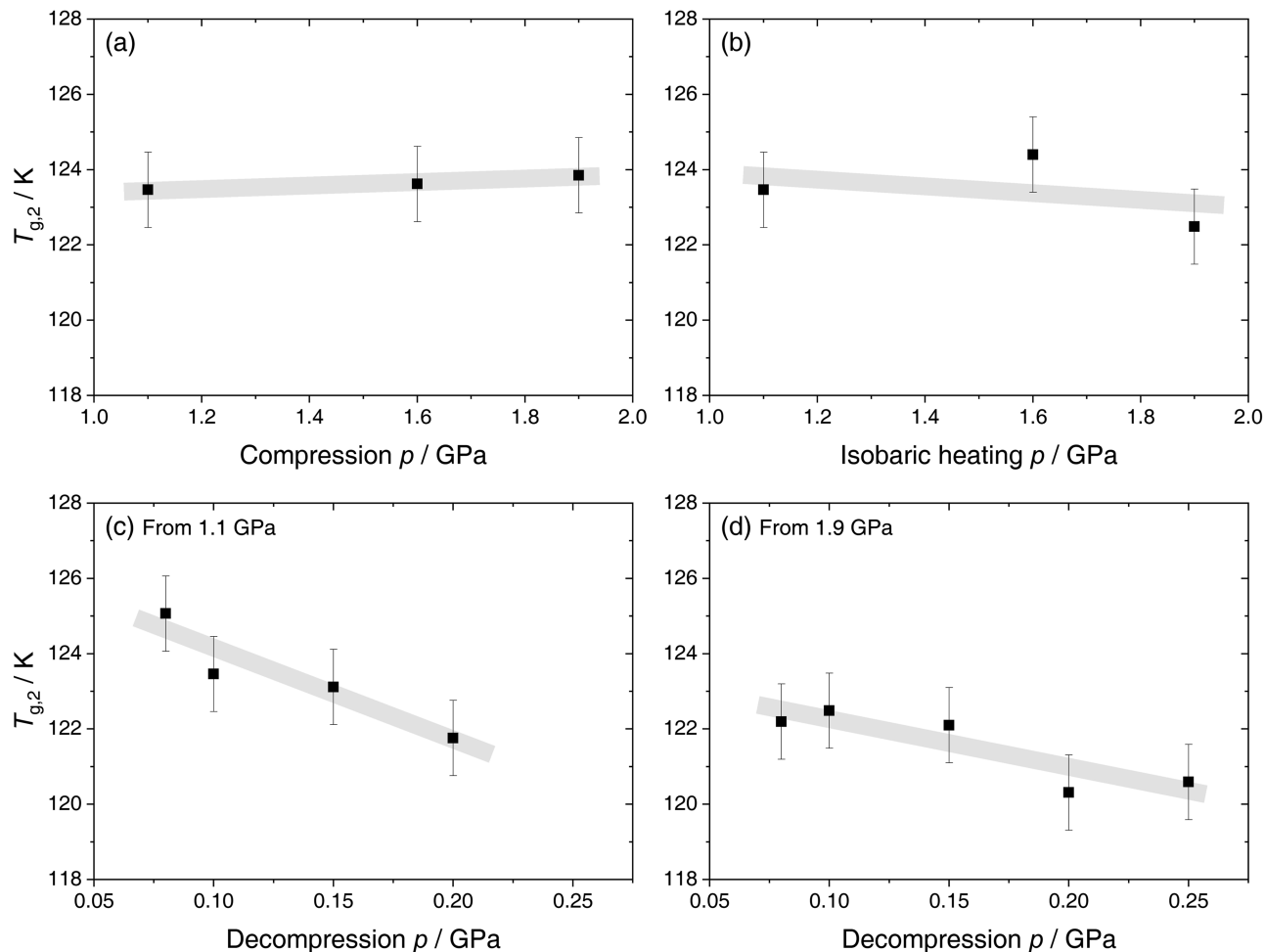


**FIG. 6.** (a)–(d) Onset temperatures of the glass-to-liquid transition from HDA  $\rightarrow$  HDL at 1 bar in d-HGW samples produced via the routes (a)–(d) in Fig. 1. The broad gray lines are guides to the eye.

upon heating at 1 bar. As a result, this seeded HDA displays no spike and also lower thermal stability toward LDA. This seems to occur more frequently in samples pressure-annealed at 1.1 GPa where the spike is never observed in 0.08 GPa and rarely observed in 0.10 GPa samples. Samples treated at 1.9 GPa, on the other hand, show a clear spike at a decompression pressure of 0.10 GPa and even the hint of a spike at 0.08 GPa. We think that this signifies lower probability of LDA nucleation during the decompression process in the samples treated at 1.9 GPa. This attenuated nucleation does not only allow us to observe a spike in samples decompressed to very low pressures but also lifts their  $T_{\text{ons}}$  considerably.

### Onset, width, and heat capacity change

We will now turn our attention to the impact of the preparation history on onset  $T_{g,2}$ , width  $\Delta T_{g,2}$ , and heat capacity increase  $\Delta c_p$  at the glass-to-liquid transition (Figs. 6–8). In an earlier work, a  $T_{g,2}$  of  $116 \pm 2$  K was reported.<sup>34</sup> Note that here we use  $30 \text{ K min}^{-1}$

rather than  $10 \text{ K min}^{-1}$ , leading to a correction of  $\sim 3\text{--}4$  K [see the [supplementary material](#) (Fig. S2)]. That is, all temperatures reported here need to be corrected down by 3–4 K when compared to the earlier work. The onset temperatures  $T_{g,2}$  shown in Figs. 6(a) and 6(b) are hardly affected by variations in the first or second preparation step and remain around  $123 \pm 1$  K. However, in Figs. 6(c) and 6(d), we observe that variation of the third step has an effect: decreasing the pressure at which samples are quenched in the decompression process at 140 K leads to an increase in  $T_{g,2}$ . At first glance, this observation might be surprising and in contradiction to our earlier studies showing  $T_{g,2}$  to increase with increasing pressure.<sup>54</sup> On second thought, there is no contradiction, though. While we have measured  $T_{g,2}$  as a function of pressure in our earlier work, we here measure all  $T_{g,2}$ 's at ambient pressure and probe the fictive temperature of the glass, i.e., we probe how far the glass is from equilibrium. For instance, excess entropy or enthalpy is a measure of how far a glass is from its ideal glassy state. That is, the observation of increase rather than decrease with pressure in Figs. 6(c) and 6(d)

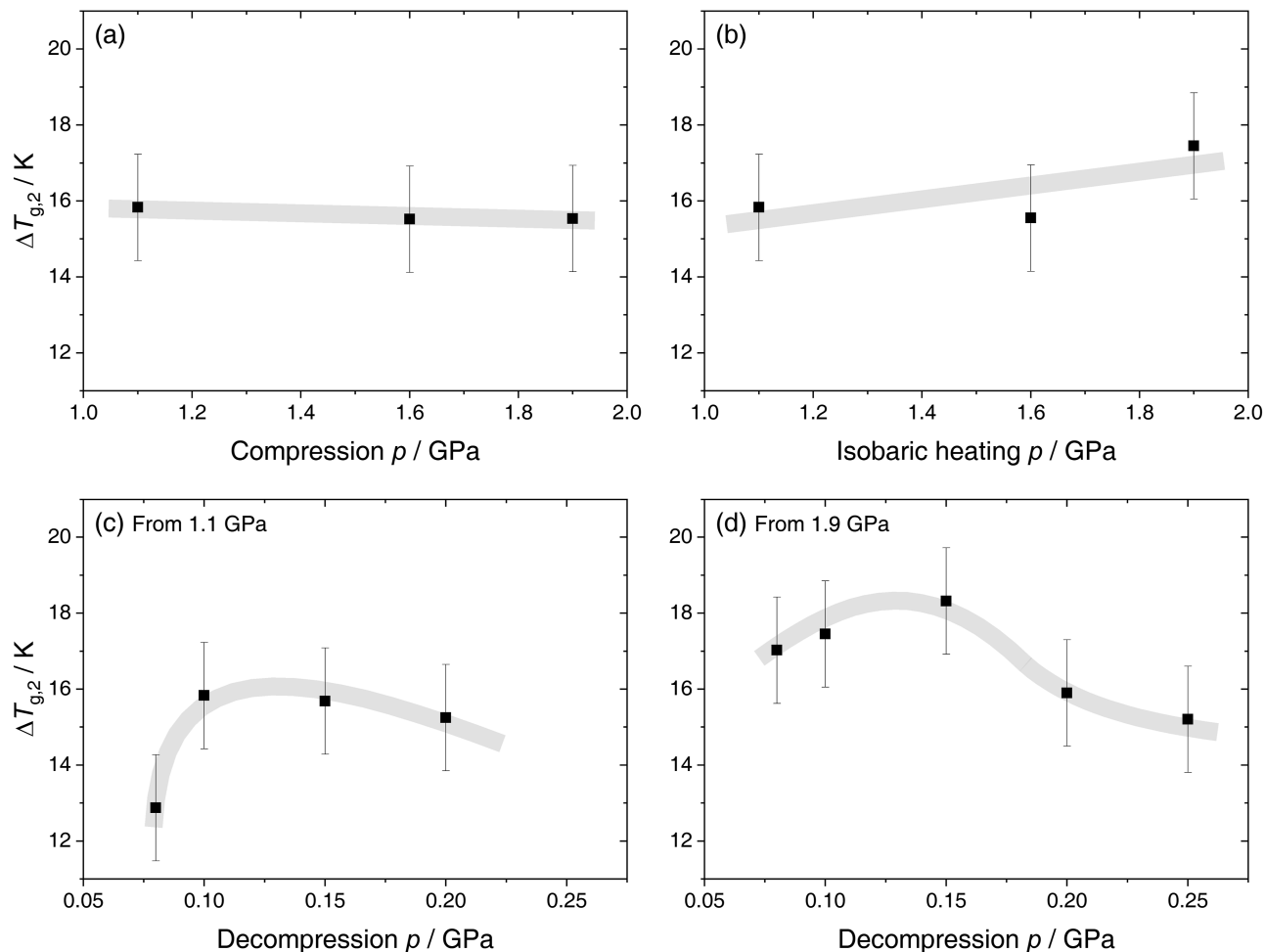


**FIG. 7.** (a)–(d) Width of the HDA  $\rightarrow$  HDL transition including a spike-like feature for d-HGW samples prepared according to Figs. 1(a)–1(d). The gray lines are added as guides to the eye. Error bars are estimated by adding the errors of the HDA  $\rightarrow$  HDL and HDA/HDL  $\rightarrow$  LDA onset temperatures using Gaussian error propagation.

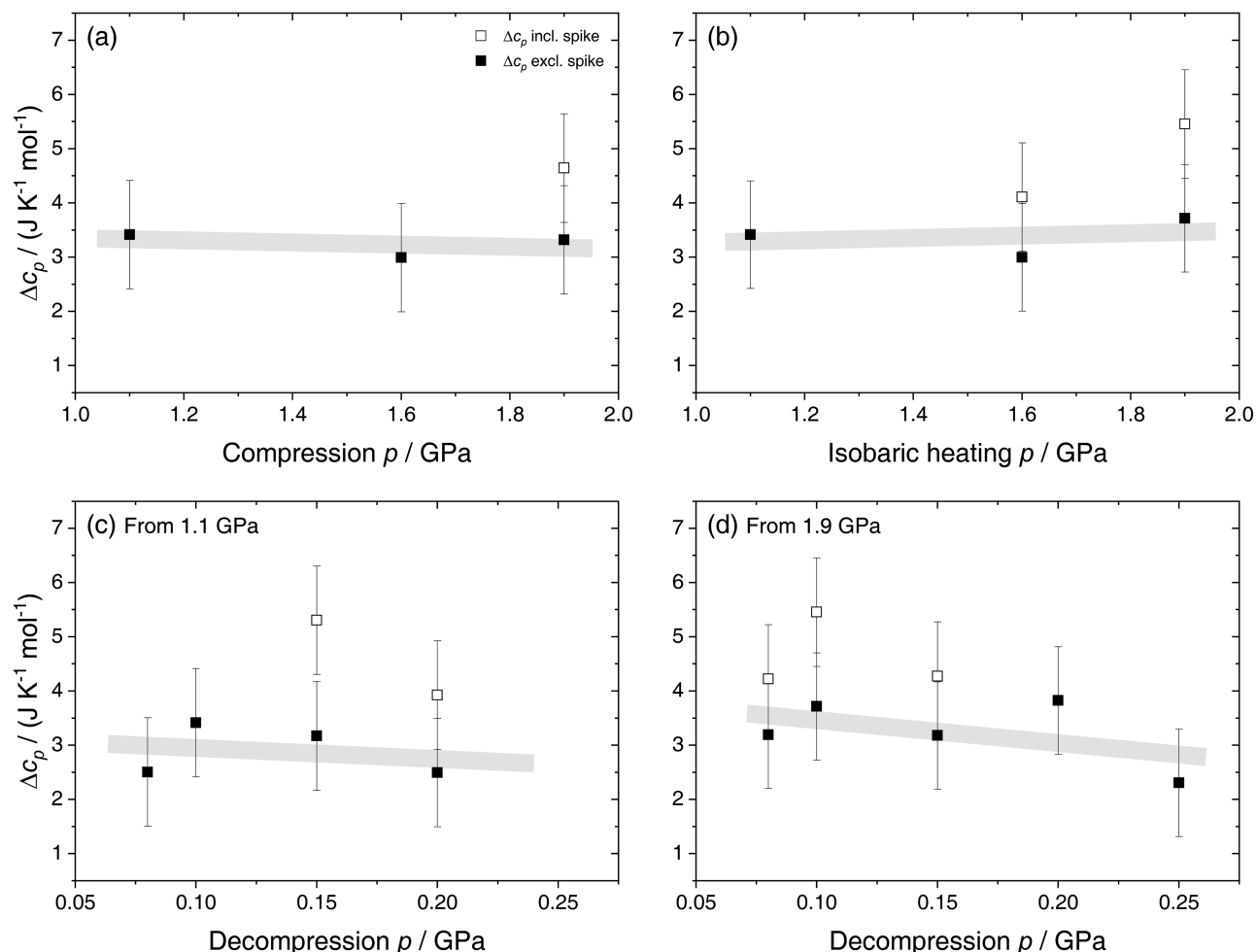


**FIG. 8.** (a)–(d) Heat capacity differences during the HDA  $\rightarrow$  HDL transition in d-HGW prepared via the routes (a)–(d) displayed in Fig. 1. Filled symbols represent heat capacity increases without spike and empty symbols the heat capacity increases with spike. Broad gray lines are added as guides to the eye.

merely indicates that the sample decompressed to 0.25 GPa/140 K has a fictive temperature different from the sample decompressed to 0.10 GPa/140 K after quench-recovery to 1 bar/77 K. In glass physics, a low glass transition temperature is usually associated with a more stable glass, i.e., one with low fictive temperature, and excess entropy/enthalpy with respect to the corresponding crystalline phase and the ideal glass.<sup>49</sup> On comparing Figs. 6(c) and 6(d), it is evident that the samples annealed previously at 1.9 GPa feature a lower  $T_{g,2}$  (and hence fictive temperature) than the ones annealed at 1.1 GPa, where the difference is most obvious at 0.08 GPa. This means that samples previously annealed at 1.9 GPa remain (meta)stable even after decompression to 0.08 GPa, whereas samples annealed at 1.1 GPa are close to instability. As demonstrated earlier by Tonaer *et al.*<sup>64</sup>, the reason for this is the growth of LDA nuclei that takes place in samples at <0.15 GPa/140 K. This growth is avoided in samples annealed previously at 1.9 GPa because LDA nuclei are avoided in this step. Consequently, HDA samples annealed at temperatures but also the highest thermal stability against the

polyamorphic transition to LDA. For samples decompressed to only 0.20 GPa, there is barely any difference between Figs. 6(c) and 6(d) because LDA growth does not take place for thermodynamic reasons—HDA is more stable than LDA. At <0.15 GPa, LDA becomes more and more stable compared to HDA so that LDA may grow if nuclei are present.

We emphasize that the goal of decreasing the glass transition temperature alone is not satisfactory if the resulting glass is only stable toward the crystalline phase but not toward LDA. Ideally,  $T_{g,2}$  would be as low as possible and  $T_{\text{ons}}$  of the polyamorphic transition as high as possible in order to maximize the range where the liquid can be studied. To investigate this issue, the width  $\Delta T_{g,2}$  of the second glass transition is calculated by subtracting  $T_{\text{ons}}$  of the HDA  $\rightarrow$  LDA transition (Fig. 3) from  $T_{g,2}$  (Fig. 6) and depicted in Fig. 7. The width represents the transformation range where the glass (HDA) gradually transforms into the supercooled liquid (HDL). It can serve as a qualitative criterion for the fragility of the liquid since a broad glass transition, i.e., large width, implies a strong nature of

the liquid.<sup>49</sup> In general,  $\Delta T_{g,2}$  exhibits a large variety, ranging from 13 to 18 K (including the spike feature). It loosely follows the behavior of  $T_{\text{ons}}$  of the polymorphic transition demonstrated in Fig. 3. The most pronounced effect on  $\Delta T_{g,2}$  is again found upon varying the end pressure of decompression. Annealing HDA at 1.9 GPa not only lifts its transition temperature to LDA but also raises the width of the glass transition to 18 K when decompressing to 0.15 GPa. This is especially striking considering that HDA treated at 1.1 GPa displays a width  $\Delta T_{g,2}$ , which is up to 5 K smaller. That is, the preparation procedure involving annealing at 1.9 GPa opens the window to study HDA above its glass transition temperature significantly and allows us to access the deeply supercooled liquid from the genuine glassy state with much less LDA nuclei than in samples previously studied after annealing at 1.1 GPa. The best, most genuine, and most stable HDA samples identified in this study are HDA samples annealed at 1.9 GPa to 175 K and decompressed at 140 K to 0.15 or 0.10 GPa. Even when the temperature range of the spike (around 3 K broad) is neglected, it is around 15 K broad. For comparing its fragility to other liquids, the width is scaled by the glass transition temperature,  $\Delta T_{g,2}/T_{g,2} = 15/122$ . This demonstrates that the second glass transition is exceptionally broad and characteristic of a strong liquid. In fact, it is even broader than for LDL ( $\Delta T_{g,1}/T_{g,1} = 12/136^{24}$ ), the benchmark case of a strong liquid, although this glass transition is far from complete due to intervening crystallization. Still, we corroborate the claim by Amann-Winkel *et al.*<sup>34</sup> of HDL at 1 bar being a strong rather than a fragile liquid.

Finally, we examine the size of the heat capacity increase  $\Delta c_p$  at the second glass transition as calculated by subtracting the  $c_p$  value at  $T_{\text{ons}}$  of the transformation to LDA and the value at  $T_{g,2}$  (see Fig. 8). Note that the comparatively large error bars result from the thermal drift in the calorimetry signal prior to the ice melting endotherm, which adds some uncertainty to the area of the melting endotherm [see the [supplementary material](#) (Fig. S1)]. This thermal drift only occurs for d-HGW but not for any other ice sample studied in our instrument, e.g., HDA made via pressure-induced amorphization, ice XII or ice XIX. Naturally, this limits the accuracy of our results to some extent and absolute values should be treated with caution. Nonetheless, we can use the extracted  $\Delta c_p$  to compare the samples with one another. In general,  $\Delta c_p$  of our samples ranges between 2.5 and 5.5 J K<sup>-1</sup> mol<sup>-1</sup>. A larger width of the glass transition (i.e., a larger window of HDL observation) correlates with the largest  $\Delta c_p$ . The sample annealed at 1.1 GPa and decompressed to 0.08 GPa shows only 2.5 J K<sup>-1</sup> mol<sup>-1</sup>, while the most stable and best sample identified above, the one annealed at 1.9 GPa and decompressed to 0.10 GPa, shows 5.5 J K<sup>-1</sup> mol<sup>-1</sup>. The doubling of  $\Delta c_p$  is due to the occurrence of the spike, which contributes significantly to  $\Delta c_p$ . Indeed, the heat capacity increase in all samples stays around  $3 \pm 1$  J K<sup>-1</sup> mol<sup>-1</sup> when subtracting the spike (see the filled symbols in Fig. 8). A constant increase in heat capacity (within experimental error and not including possible over- or undershoots) regardless of preparation history is the expected behavior during a glass-to-liquid transition. We believe that this is strong evidence that the spike is a separate event unrelated to the glass-to-liquid transition of HDA, specifically LDA nucleation in samples that were free of LDA nuclei prior to the DSC scan. This furthermore rules out the possibility of it being related to the unlocking of translational modes. The translational modes are unlocked at the glass transition onset  $T_{g,2}$ , near 122 K.

## SUMMARY AND OUTLOOK

In summary, we studied the preparation history dependence of HDA produced from vitrified droplets by subjecting it to different pressure-annealing protocols. The main advantage of vitrified droplets as the starting material is that compared to previous studies no crystalline phases are encountered at any time during our preparation protocols. After quenching at a variety of  $p$ - $T$  points, the samples were recovered to 1 bar where thermal analysis was performed. We report differences in both the behavior during the second glass transition as well as in thermal stability toward the exothermic polyamorphic transition to LDA. The clearest differences appear upon varying the decompression pressure at 140 K. Decreasing the decompression pressure gradually from 0.25 to 0.10 GPa increases the transformation temperature to LDA. This is linked to HDA relaxing toward its (metastable) equilibrium state. Decreasing the decompression further to 0.08 GPa, decreases the transformation temperature to LDA again, which is attributed to LDA nucleation during the decompression process in accordance with the work of Tonauer *et al.*<sup>64</sup> Nucleation occurs less frequently in HDA treated at 1.9 GPa compared to the one treated at 1.1 GPa, leading to slightly more stable samples. That is, the thermally most stable HDA is identified to be the one annealed at 1.9 GPa and decompressed to 0.15–0.10 GPa at 140 K with HGW as a starting material. This preparation protocol differs from the one used in earlier work to study water's second glass transition<sup>34,47</sup> and supersedes it as the best protocol to study the genuine glassy HDA state of the highest thermodynamic and kinetic stability. This new protocol leads to the lowest onset temperature of the second glass transition (HDA to HDL)  $T_{g,2}$  identified in the present study, which is indicative of the lowest fictive temperature and smallest excess entropy of HDA. The highest thermal stability against the polyamorphic transition and the lowest  $T_{g,2}$  result in the largest width of the glass transition encountered in literature, where the width reaches 18 K (including spike-like feature) or 15 K (excluding spike-like feature) for the best preparation protocols. Our protocol expands this window by about 4 K when compared to the previous study by Amann-Winkel *et al.*<sup>34</sup> The change in heat capacity at the glass-to-liquid transition can be up to 5.5 J K<sup>-1</sup> mol<sup>-1</sup> including the spike but remains constant at  $3 \pm 1$  J K<sup>-1</sup> mol<sup>-1</sup> regardless of preparation protocols used here when not considering the spike as part of the glass-to-liquid transition. We suggest that the spike relates to nucleation of LDL, where the nucleation barrier is at the origin of the endothermic, spike-like feature. Observation of LDL nucleation, i.e., the spike, in the calorimetry scan necessitates that no LDA nucleates during the decompression procedure. Growth of LDA nuclei under high-pressure conditions is avoided only for samples that are decompressed to  $p \geq 0.15$  GPa or for samples annealed previously at 1.9 GPa. The former avoids LDA growth by staying away from the pressure-range, where LDA is thermodynamically more stable than HDA. However, if the relaxation (=decompression) pressure is too high (above 0.20 GPa), endothermic LDL nucleation is preceded by exothermic enthalpy relaxation and the polyamorphic transition. Consequently, the spike is no longer observed. The latter avoids LDA/LDL growth by removing all potential LDA/LDL nucleation sites at 1.9 GPa. This latter strategy is the only viable strategy to make HDL samples, i.e., ultraviscous liquid samples starting from HDA at 1 bar. Consequently, our systematic DSC study reveals protocols that are suitable to make HDL from vitrified and pressurized



liquid droplets, where both crystallization and the polyamorphic transformation are avoided—allowing for characterization of HDL up to higher temperatures (and for longer times at the same temperature). The present study shows that the thawing of HDA at 1 bar is a complex multistep process, which is remarkably sensitive to the preparation path chosen. Our idea that HDA/HDL transform to LDA/LDL at 1 bar via nucleation and growth resonates well with the idea that water is composed of two distinct liquids that are connected via a first-order transition. The knowledge generated in our work about the impact of the preparation history on nucleation paves the way for understanding of the potential liquid–liquid transition at 140 K reported in 2009 by Winkel *et al.*,<sup>33</sup> where the mechanism may either by spinodal-like decomposition (if there are LDL-nuclei present beforehand) or nucleation and growth (if there are none present beforehand). According to our findings, the LLT conjectured in the work by Winkel *et al.* did proceed through growth of pre-existing low-density nuclei. Repeating their study with samples made from vitrified droplets annealed at 1.9 GPa might change the mechanism to a genuine nucleation and growth mechanism, making the case for the LLT to involve nucleation and of one liquid (LDL) within the matrix of another (HDL), both of composition H<sub>2</sub>O. This also involves the build-up of interfaces between two distinct liquids—making the case for the LLT being a first-order transition. We hope that our work sparks sufficient interest to stimulate the use of powerful tools probing structure, such as neutron diffraction and x-ray free electron lasers, for the most stable HDL samples reported in this work.

## SUPPLEMENTARY MATERIAL

The [supplementary material](#) shows thermograms of LDA made from d-HGW, d-HGW heated at different rates, and HDA made via pressure-induced amorphization of ice I. Furthermore, data on latent heat release during the polyamorphic transition are displayed.

## ACKNOWLEDGMENTS

J.B. is a recipient of a DOC fellowship of the Austrian Academy of Sciences (ÖAW) and of an Early Stage grant of the University of Innsbruck provided by the vice rector of research.

## AUTHOR DECLARATIONS

### Conflict of Interest

The authors have no conflicts to disclose.

## Author Contributions

**Johannes Bachler:** Conceptualization (equal); Formal analysis (lead); Funding acquisition (supporting); Investigation (lead); Methodology (equal); Writing – original draft (lead); Writing – review & editing (supporting). **Johannes Giebelmann:** Investigation (supporting); Methodology (supporting); Writing – review & editing (supporting). **Katrin Amann-Winkel:** Investigation (supporting); Writing – review & editing (supporting). **Thomas Loerting:**

Conceptualization (equal); Formal analysis (equal); Funding acquisition (lead); Investigation (supporting); Methodology (equal); Project administration (lead); Resources (lead); Supervision (lead); Writing – original draft (supporting); Writing – review & editing (lead).

## DATA AVAILABILITY

The data that support the findings of this study are available from the corresponding author upon reasonable request.

## REFERENCES

- 1 M. R. El-Maarry, O. Groussin, N. Thomas, M. Pajola *et al.*, *Science* **355**, 1392 (2017).
- 2 T. Encrenaz, *Annu. Rev. Astron. Astrophys.* **46**, 57 (2008).
- 3 P. Jenniskens and D. F. Blake, *Science* **265**, 753 (1994).
- 4 P. G. Debenedetti, *J. Phys.: Condens. Matter* **15**, R1669 (2003).
- 5 P. H. Handle, T. Loerting, and F. Sciortino, *Proc. Natl. Acad. Sci. U. S. A.* **114**, 13336 (2017).
- 6 P. Gallo, K. Amann-Winkel, C. A. Angell, M. A. Anisimov *et al.*, *Chem. Rev.* **116**, 7463 (2016).
- 7 P. Gallo, J. Bachler, L. E. Bove, R. Böhmer *et al.*, *Eur. Phys. J. E* **44**, 143 (2021).
- 8 R. J. Speedy, *J. Phys. Chem.* **86**, 982 (1982).
- 9 P. H. Poole, F. Sciortino, U. Essmann, and H. E. Stanley, *Nature* **360**, 324 (1992).
- 10 L. P. N. Rebelo, P. G. Debenedetti, and S. Sastry, *J. Chem. Phys.* **109**, 626 (1998).
- 11 S. Sastry, P. G. Debenedetti, F. Sciortino, and H. E. Stanley, *Phys. Rev. E* **53**, 6144 (1996).
- 12 J. C. Palmer, P. H. Poole, F. Sciortino, and P. G. Debenedetti, *Chem. Rev.* **118**, 9129 (2018).
- 13 P. G. Debenedetti, F. Sciortino, and G. H. Zerze, *Science* **369**, 289 (2020).
- 14 H. Kanno, R. J. Speedy, and C. A. Angell, *Science* **189**, 880 (1975).
- 15 H. Laksmono, T. A. McQueen, J. A. Sellberg, N. D. Loh *et al.*, *J. Phys. Chem. Lett.* **6**, 2826 (2015).
- 16 T. Loerting, M. Bauer, I. Kohl, K. Watschinger, K. Winkel, and E. Mayer, *J. Phys. Chem. B* **115**, 14167 (2011).
- 17 D. T. Bowron, J. L. Finney, A. Hallbrucker, I. Kohl, T. Loerting, E. Mayer, and A. K. Soper, *J. Chem. Phys.* **125**, 194502 (2006).
- 18 J. L. Finney, A. Hallbrucker, I. Kohl, A. K. Soper, and D. T. Bowron, *Phys. Rev. Lett.* **88**, 225503 (2002).
- 19 E. F. Burton and W. F. Oliver, *Proc. R. Soc. London, Ser. A* **153**, 158–166 (1935).
- 20 P. Brüggeller and E. Mayer, *Nature* **288**, 569 (1980).
- 21 E. Mayer, *J. Phys. Chem.* **58**, 663 (1985).
- 22 O. Mishima, L. D. Calvert, and E. Whalley, *Nature* **314**, 76 (1985).
- 23 G. P. Johari, A. Hallbrucker, and E. Mayer, *Nature* **330**, 552 (1987).
- 24 I. Kohl, L. Bachmann, A. Hallbrucker, E. Mayer, and T. Loerting, *Phys. Chem. Chem. Phys.* **7**, 3210 (2005).
- 25 I. Kohl, L. Bachmann, E. Mayer, A. Hallbrucker, and T. Loerting, *Nature* **435**, E1 (2005).
- 26 W. Hage, A. Hallbrucker, E. Mayer, and G. P. Johari, *J. Chem. Phys.* **100**, 2743 (1994).
- 27 O. Mishima, *Nature* **384**, 546 (1996).
- 28 O. Mishima, L. D. Calvert, and E. Whalley, *Nature* **310**, 393 (1984).
- 29 S. Klotz, T. Strässle, A. M. Saitta, G. Rouse, G. Hamel, R. J. Nelmes, J. S. Loveday, and M. Guthrie, *J. Phys.: Condens. Matter* **17**, S967 (2005).
- 30 Y. P. Handa, O. Mishima, and E. Whalley, *J. Chem. Phys.* **84**, 2766 (1986).
- 31 R. J. Nelmes, J. S. Loveday, T. Strässle, C. L. Bull, M. Guthrie, G. Hamel, and S. Klotz, *Nat. Phys.* **2**, 414 (2006).
- 32 K. Winkel, M. S. Elsaesser, E. Mayer, and T. Loerting, *J. Chem. Phys.* **128**, 044510 (2008).
- 33 K. Winkel, E. Mayer, and T. Loerting, *J. Phys. Chem. B* **115**, 14141 (2011).

- <sup>34</sup>K. Amann-Winkel, C. Gainaru, P. H. Handle, M. Seidl, H. Nelson, R. Böhmer, and T. Loerting, *Proc. Natl. Acad. Sci. U. S. A.* **110**, 17720 (2013).
- <sup>35</sup>K. H. Kim, K. Amann-Winkel, N. Giovambattista, A. Späh *et al.*, *Science* **370**, 978 (2020).
- <sup>36</sup>L. Kringle, W. A. Thornley, B. D. Kay, and G. A. Kimmel, *Science* **369**, 1490 (2020).
- <sup>37</sup>O. Mishima, *J. Chem. Phys.* **133**, 144503 (2010).
- <sup>38</sup>K. H. Kim, A. Späh, H. Pathak, F. Perakis *et al.*, *Science* **358**, 1589 (2017).
- <sup>39</sup>H. Pathak, A. Späh, N. Esmaildoost, J. A. Sellberg *et al.*, *Proc. Natl. Acad. Sci. U. S. A.* **118**, e2018379118 (2021).
- <sup>40</sup>O. Mishima and H. E. Stanley, *Nature* **392**, 164 (1998).
- <sup>41</sup>J. S. Tse, D. D. Klug, C. A. Tulk, I. Swainson *et al.*, *Nature* **400**, 647 (1999).
- <sup>42</sup>G. P. Johari, *Phys. Chem. Chem. Phys.* **2**, 1567 (2000).
- <sup>43</sup>A. I. Kolesnikov, V. V. Sinitsyn, E. G. Ponyatovsky, I. Natkaniec, and L. S. Smirnov, *Phys. Rev. B* **213–214**, 474 (1995).
- <sup>44</sup>J.-C. Li and P. Jenniskens, *Planet. Space Sci.* **45**, 469 (1997).
- <sup>45</sup>J. J. Shephard, S. Ling, G. C. Sosso, A. Michaelides, B. Slater, and C. G. Salzmann, *J. Phys. Chem. Lett.* **8**, 1645 (2017).
- <sup>46</sup>K. Amann-Winkel, R. Böhmer, F. Fujara, C. Gainaru, B. Geil, and T. Loerting, *Rev. Mod. Phys.* **88**, 011002 (2016).
- <sup>47</sup>V. Fuentes-Landete, L. J. Plaga, M. Keppler, R. Böhmer, and T. Loerting, *Phys. Rev. X* **9**, 011015 (2019).
- <sup>48</sup>J. Bachler, J. Giebelmann, and T. Loerting, *Proc. Natl. Acad. Sci. U. S. A.* **118**, e2108194118 (2021).
- <sup>49</sup>C. A. Angell, *Chem. Rev.* **102**, 2627 (2002).
- <sup>50</sup>T. Atake and C. A. Angell, *J. Phys. Chem.* **83**, 3218 (1979).
- <sup>51</sup>N. Giovambattista, T. Loerting, B. R. Lukanov, and F. W. Starr, *Sci. Rep.* **2**, 390 (2012).
- <sup>52</sup>O. Mishima, *J. Chem. Phys.* **121**, 3161 (2004).
- <sup>53</sup>O. Andersson, *Proc. Natl. Acad. Sci. U. S. A.* **108**, 11013 (2011).
- <sup>54</sup>M. Seidl, M. S. Elsaesser, K. Winkel, G. Zifferer, E. Mayer, and T. Loerting, *Phys. Rev. B* **83**, 100201 (2011).
- <sup>55</sup>P. H. Handle and T. Loerting, *Phys. Rev. B* **93**, 064204 (2016).
- <sup>56</sup>I. Kohl, E. Mayer, and A. Hallbrucker, *Phys. Chem. Chem. Phys.* **3**, 602 (2001).
- <sup>57</sup>C. M. Tonauer, M. Bauer, and T. Loerting, *Phys. Chem. Chem. Phys.* **24**, 35 (2022).
- <sup>58</sup>K. Winkel, M. Bauer, E. Mayer, M. Seidl, M. S. Elsaesser, and T. Loerting, *J. Phys.: Condens. Matter* **20**, 494212 (2008).
- <sup>59</sup>J. N. Stern and T. Loerting, *Phys. Chem. Chem. Phys.* **20**, 12589 (2018).
- <sup>60</sup>J. N. Stern, M. Seidl-Nigsch, and T. Loerting, *Proc. Natl. Acad. Sci. U. S. A.* **116**, 9191 (2019).
- <sup>61</sup>J. Bachler, V. Fuentes-Landete, D. A. Jahn, J. Wong, N. Giovambattista, and T. Loerting, *Phys. Chem. Chem. Phys.* **18**, 11058 (2016).
- <sup>62</sup>G. W. H. Höhne, W. F. Hemminger, and H.-J. Flammersheim, *Differential Scanning Calorimetry* (Springer, Berlin, Heidelberg, 2003), ISBN: 978-3-540-00467-7.
- <sup>63</sup>K. Winkel, “Study of amorphous-amorphous transitions in water,” Ph.D. thesis, Verlag Dr. Hut, 2009.
- <sup>64</sup>C. M. Tonauer, M. Seidl-Nigsch, and T. Loerting, *J. Phys.: Condens. Matter* **30**, 034002 (2018).
- <sup>65</sup>O. Mishima, *J. Chem. Phys.* **100**, 5910 (1994).
- <sup>66</sup>G. N. Ruiz, K. Amann-Winkel, L. E. Bove, H. R. Corti, and T. Loerting, *Phys. Chem. Chem. Phys.* **20**, 6401 (2018).
- <sup>67</sup>Y. Suzuki, *Proc. Natl. Acad. Sci. U. S. A.* **119**, e2113411119 (2022).
- <sup>68</sup>F. Perakis, K. Amann-Winkel, F. Lehmkuhler, M. Sprung *et al.*, *Proc. Natl. Acad. Sci. U. S. A.* **114**, 8193 (2017).
- <sup>69</sup>T. M. Truskett, P. G. Debenedetti, S. Sastry, and S. Torquato, *J. Chem. Phys.* **111**, 2647 (1999).
- <sup>70</sup>P. H. Poole, F. Sciortino, T. Grande, H. E. Stanley, and C. A. Angell, *Phys. Rev. Lett.* **73**, 1632 (1994).
- <sup>71</sup>V. Fuentes-Landete, C. Mitterdorfer, P. Handle, G. Ruiz *et al.*, in *Proceedings of the International School of Physics “Enrico Fermi”* (IOS Press, 2015), p. 173.